

High-Dimensional Disorder-Driven Phenomena in Weyl Semimetals, Semiconductors and Related Systems

Sergey V. Syzranov^{1,2} and Leo Radzihovsky^{1,3,4}

¹Physics Department and Center for Theory of Quantum Matter, University of Colorado, Boulder, USA, CO 80309; email: sergey.syzranov@googlemail.com

²Joint Quantum Institute, NIST/University of Maryland, College Park, USA, MD 20742

³JILA, University of Colorado, Boulder, USA, CO 80309

⁴KITP, University of California, Santa-Barbara, USA, CA 93106

Ann. Rev. Cond. Mat. Phys. 2017. 9:1–26

This article's doi:
10.1146/((article doi))

Copyright © 2017 by Annual Reviews.
All rights reserved

Keywords

localisation, phase transitions, disordered systems, Dirac semimetals

Abstract

It is commonly believed that a non-interacting disordered electronic system can undergo only the Anderson metal-insulator transition. It has been suggested, however, that a broad class of systems can display disorder-driven transitions distinct from Anderson localisation that have manifestations in the disorder-averaged density of states, conductivity and other observables. Such transitions have received particular attention in the context of recently discovered 3D Weyl and Dirac materials but have also been predicted in cold-atom systems with long-range interactions, quantum kicked rotors, and all sufficiently high-dimensional systems. Moreover, such systems exhibit unconventional behaviour of Lifshitz tails, energy-level statistics, and ballistic-transport properties. Here we review recent progress and the status of results on non-Anderson disorder-driven transitions and related phenomena.

Contents

1. INTRODUCTION	2
2. DISORDER-INDUCED PHENOMENA IN HIGH DIMENSIONS	5
2.1. Phenomenological argument for a transition near nodes and band edges	5
2.2. Self-consistent Born approximation ($N = \infty$ approach)	6
2.3. Renormalisation-group analysis	7
2.4. Non-Anderson vs. Anderson transitions	8
2.5. Related phenomena in disorder-free interacting systems	9
3. PHYSICAL OBSERVABLES NEAR THE TRANSITION	10
3.1. Critical exponents	10
3.2. Density of states	11
3.3. Mobility threshold	11
3.4. Conductivity	12
3.5. Multifractality	14
4. FINITE-SIZE EFFECTS IN HIGH DIMENSIONS	15
4.1. Level discreteness and ballistic transport in disordered systems	15
4.2. Conductance of finite semimetallic samples	16
5. RARE-REGION EFFECTS	17
5.1. Lifshitz tails	18
5.2. Phase transition vs. sharp crossover	19
6. POTENTIAL FOR EXPERIMENTAL REALISATION	19
6.1. Weyl and 3D Dirac semimetals	19
6.2. 1D and 2D arrays of ultracold trapped ions	20
6.3. Chiral superconductors	21
6.4. Quantum kicked rotors	21
6.5. Numerical simulations in high dimensions	22
7. OPEN QUESTIONS AND FUTURE PROBLEMS	22

1. INTRODUCTION

Quenched disorder, such as impurities, vacancies, and dislocations, is inherently present in all solid-state systems. It determines conduction, affects the properties of phases and their associated phase transitions, and leads to new phases of matter.

The amount of quenched disorder often determines the difference between metals and insulators, respectively materials with finite and zero conductivity at zero temperature. When the amount of disorder is increased, a metal can turn into an insulator due to the Anderson localisation(1) of electron states at the Fermi surface. This insulating behaviour at strong disorder persists, in particular, in the presence of sufficiently weak interactions(2).

Interest in localisation phenomena and the other effects of disorder continues to be fuelled by discoveries of new materials with non-trivial topologies and quasiparticle band structures, including d -wave superconductors, graphene, and 3D Dirac and Weyl semimetals.

The novel band structures and topological properties in such materials require a reexamination of transport and thermodynamic phenomena. While in systems with large electron density (with the Fermi level deep inside the band), one can apply the conventional treatment based on an effective constant density of states, elastic scattering rate, electron mass etc.(3, 4, 5), such an approach fails completely when the density of states vanishes, which

occurs near nodes (e.g., in graphene or Weyl semimetals) and band edges. In these regimes, which are the subject of this review, a qualitatively different treatment is required and new phenomena are expected and indeed found.

For example, under certain approximations it was demonstrated(6, 7) more than 30 years ago that a three-dimensional (3D) system with Dirac quasiparticle dispersion exhibits a novel disorder-driven transition between two phases, with zero and finite densities of states (DoS), at the Dirac node. This contrasts qualitatively with the Anderson localisation transition, commonly believed to be the only possibility for a non-interacting disordered system, where the DoS exhibits no interesting features through the transition.

Interest in the prediction of this unconventional (non-Anderson) disorder-driven phase transition has been revived recently by the advent of 3D Dirac(8, 9, 10, 11) and Weyl(12, 13, 14, 15, 16, 17) semimetals (WSMs). Extensive theoretical and numerical studies [see, e.g., Refs. (18, 19, 20, 21, 22, 23, 24, 25, 26, 27, 28, 29, 30, 31, 32, 33, 34, 35, 36, 37, 38, 39)] over the last several years have been directed at exploring the properties of such transitions and the behaviour of physical observables in Dirac and Weyl systems. Although the density of states never exactly vanishes(40, 41, 42, 43, 24), in contrast with the expectations of the pioneering studies(6, 7), this nevertheless does not preclude a singular (non-analytic) behaviour near a critical value of the disorder strength on top of a smooth non-zero background.

Alternatively, it has been argued [see, e.g., Refs. (34) and (39)] that the proposed non-Anderson transition may in fact be a sharp crossover, which is rounded off in a small region in the vicinity of the putative critical point by rare-region effects, as we will discuss in Section 5. In most of this review, however, we will not distinguish between such a sharp crossover and a true disorder-driven phase transition and refer to the proposed critical point as “non-Anderson disorder-driven transition”. Although the DoS is not an order parameter

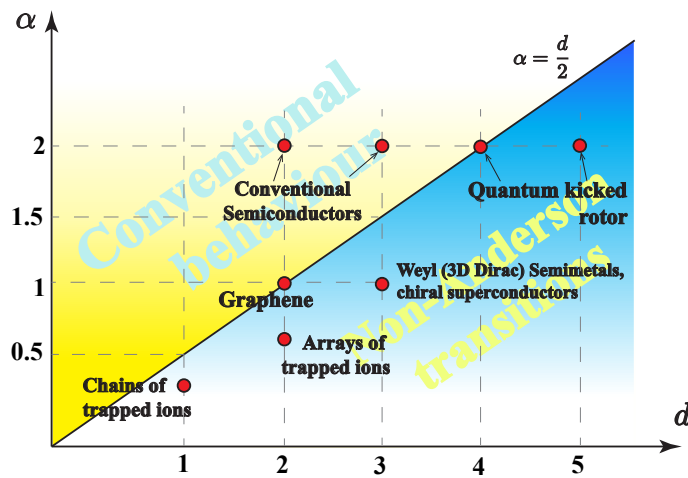


Figure 1

Examples of systems with the power-law quasiparticle dispersion $\epsilon_{\mathbf{k}} \propto k^\alpha$. Systems in high dimensions, $d > 2\alpha$, exhibit non-Anderson disorder-driven transitions.

for this transition in a strict sense, it can be used to distinguish the phases under certain approximations; the DoS is suppressed for disorder strengths weaker than a critical value and grows rapidly for stronger disorder. In the case this non-Anderson transition is a true

phase transition, which is currently not established, the phases may be distinguished by a qualitative change in the behaviour of correlation functions of physical observables.

It has been demonstrated recently(23, 24) that such a transition in 3D Dirac and Weyl materials is a special case of a more general non-Anderson disorder-driven transition that occurs in all systems in sufficiently high dimensions, summarised by a "phase diagram" with a number of examples in Fig. 1. In particular, such transitions take place in all systems with the power-law quasiparticle dispersion $\epsilon_{\mathbf{k}} \propto k^\alpha$ in dimensions $d > 2\alpha$ (referred to in this review as "high dimensions"), as illustrated in Fig. 1. As we discuss in this review, the best known example here, of direct experimental relevance, is 3D Dirac materials ($\alpha = 1$, $d = 3$), such as Dirac and Weyl semimetals and chiral superconductors. The transition has also been predicted to be realisable(44) in 1D(45, 46, 47, 48) and 2D(49) arrays of trapped ions with long-range interactions; such arrays host quasiparticles with the power-law dispersion $\epsilon_{\mathbf{k}} \propto k^\alpha$ with tunable α and thus present a flexible platform for studying the transition. Another class of systems, which allow for the observation of non-Anderson transitions, is quantum rotors kicked by perturbations with d incommensurate frequencies(50, 51, 52): such a rotor can be mapped(53, 54) onto a disordered semiconductor in dimension d and is thus expected to display a transition for $d > 4$. Quantum kicked rotors with arbitrary d may be realised in cold-atom systems and have already been demonstrated for $d = 1$ (50) and $d = 3$ (51, 52). High-dimensional disorder-driven transitions can be also studied numerically in arbitrary dimensions(55, 56, 57, 58, 59).

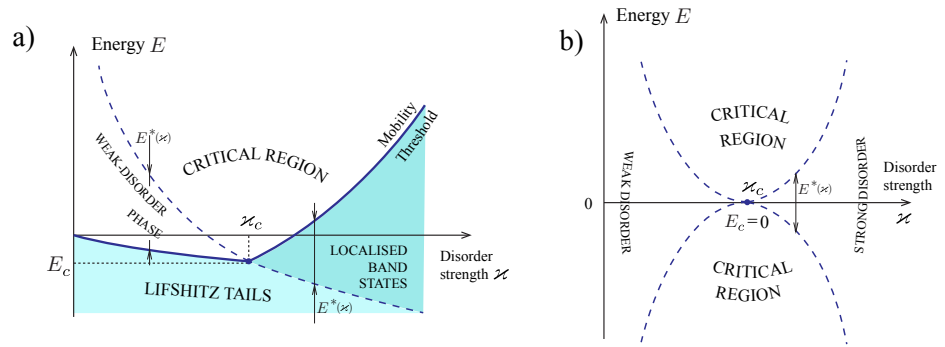


Figure 2

Phase diagram of materials that exhibit non-Anderson disorder-driven transitions: a) "high-dimensional" semiconductor in the orthogonal symmetry class, b) Weyl semimetal and 3D Dirac materials. The transition takes place at a single energy, E_c (in a WSM $E_c = 0$). In a semiconductor the transition is expected to lead to non-analytic behaviour of the mobility threshold; it is pinned to the band edge (neglecting Lifshitz tails) for subcritical disorder and grows rapidly for supercritical disorder.

This disorder-driven transition occurs for single-particle states only at one value of energy, E_c , near a node or a band edge, Fig. 2, in contrast to the Anderson localisation transition, which occurs for any energy in the band when the disorder strength is varied. This non-Anderson transition can also be accompanied by a localisation-delocalisation of the wavefunctions at the transition point, if allowed by symmetry, dimension, and topology. However, these transitions also occur in systems where localisation is forbidden by

symmetry and/or topology, such as 1D chiral chains(44) and single-node Weyl semimetals, and in systems with all states localised (e.g., systems in the orthogonal symmetry class in dimensions $d < 2$). In this case the transition manifests itself in the critical behaviour of the DoS and other observables, as discussed in detail below.

The purpose of this article is to review the properties of the unconventional non-Anderson disorder-driven transitions, the status of various results associated with them, and the possibility of their experimental observation in realistic systems.

2. DISORDER-INDUCED PHENOMENA IN HIGH DIMENSIONS

In this review we focus on the properties of d -dimensional systems described by the (single-particle) Hamiltonian

$$\hat{\mathcal{H}} = a|\mathbf{k}|^\alpha + U(\mathbf{r}), \quad (1)$$

where $\mathbf{k} = -i\partial_{\mathbf{r}}$ is the momentum operator (throughout this review we set $\hbar = 1$), $U(\mathbf{r})$ is a short-range-correlated random potential with zero average, and $\epsilon_{\mathbf{k}} = a|\mathbf{k}|^\alpha$ is the kinetic energy. In some materials the kinetic energy has an additional spin or valley structure; for instance, in graphene and Weyl semimetals $\epsilon_{\mathbf{k}} = v\mathbf{k} \cdot \hat{\boldsymbol{\sigma}}$, where $\hat{\boldsymbol{\sigma}}$ is a vector of Pauli matrices in the space of a discrete degree of freedom (e.g. spin or valley space). In most of the review we consider effects on length scales significantly longer than the correlation length of the random potential, which can thus be taken to have the delta-correlated form,

$$\langle U(\mathbf{r})U(\mathbf{r}') \rangle_{\text{dis}} = \varkappa\delta(\mathbf{r} - \mathbf{r}'), \quad (2)$$

where the delta-function is regularised by a cutoff set by the correlation length of the random potential.

2.1. Phenomenological argument for a transition near nodes and band edges

Before delving into technical details, we present a physical argument that suggests the existence of the non-Anderson disorder-driven phase transition in sufficiently high dimensions.

The effective strength of a weak random potential with a typical amplitude $U_0 \ll ar_0^{-\alpha}$ and correlation length $r_0 \ll 1/k$ can be characterised by the average of the potential over the de Broglie wavelength $2\pi/k$. According to the central limit theorem, this gives $U_{\text{rms}} \sim U_0(kr_0)^{\frac{d}{2}}$, which for low momentum states k in high dimensions $d > 2\alpha$ is always subdominant to the corresponding kinetic energy ak^α . By contrast, in low dimensions $d < 2\alpha$ an arbitrarily weak random potential always dominates at sufficiently long wavelengths, which leads, for example, to the localisation of states at the bottom of the band of a conventional semiconductor.

This strict *perturbative* argument breaks down for strong random potential, which is expected to modify the above weak-disorder state qualitatively and make the system behave similarly to a conventional semiconductor. Taken together, this thus suggests a disorder-driven transition between weak- and strong-disorder phases.

We emphasise that these arguments apply to all systems in high dimensions $d > 2\alpha$ and are not specific to Dirac materials where the transition was first suggested(6, 7). Moreover, this transition is a priori unrelated to the Anderson localisation transition or even to its existence in the system under consideration. Indeed, the above arguments apply regardless of whether disorder allows for coherent backscattering required for Anderson localisation.

Also, the physics of this high-dimensional transition is controlled by length scales shorter than the mean free path ℓ , while the properties of Anderson localisation and its existence are determined by length scales longer than ℓ (5).

2.2. Self-consistent Born approximation ($N = \infty$ approach)

We now turn to a more rigorous quantitative description of the non-Anderson transition and physical observables near it.

Born approximation. The above physical arguments are reflected in the behaviour of the elastic scattering rate $\Gamma(E)$ as a function of the particle energy E . In the leading-order perturbation theory (Born approximation) $\Gamma(E) \propto E^{\frac{d}{\alpha}-1}$. The dimensionless strength of disorder $\gamma(E) = \Gamma(E)/E \equiv [k\ell(k)]^{-1} \propto E^{\frac{d}{\alpha}-2}$ shows that in high dimensions $d > 2\alpha$ effects of weak disorder only become weaker at the bottom of the band, $E \rightarrow 0$.

By contrast, for $d < 2\alpha$ disorder cannot be treated perturbatively at low energies, which reflects, for instance, in the localisation of states near semiconductor band edges.

Self-consistent Born approximation. To treat strong disorder one can try to employ the self-consistent Born approximation (SCBA), that was used to first predict(6, 7) the transition in Dirac materials 30 years ago.

The approximation amounts to a self-consistent evaluation of the scattering rate Γ using the Green's function, e.g., $G^R = (E - \epsilon_{\mathbf{k}} + i\Gamma/2)^{-1}$, that contains the same scattering rate as a function of the disorder strength \varkappa and energy E :

$$\Gamma(\varkappa, E) = \varkappa \int \frac{d^d \mathbf{k}}{(2\pi)^d} \frac{\Gamma(\varkappa, E)}{(E - ak^\alpha)^2 + [\Gamma(\varkappa, E)]^2/4}. \quad (3)$$

Eq. (3) applies both to semiconductors with the quasiparticle dispersion $\epsilon_{\mathbf{k}} = ak^\alpha$ and to systems with dispersions that have more complicated spin or valley structures, e.g. Weyl semimetals, such that $|\epsilon_{\mathbf{k}}| = ak^\alpha$. Above for simplicity we disregard the real part of the self-energy responsible for the disorder-induced shift of the lowest energy levels.

The self-consistency equation (3) matches the saddle-point solution of the non-linear sigma-model(5). Fluctuations around the saddle-point solutions make physical observables deviate from the SCBA result. Such fluctuations, however, can be taken into account systematically via the $1/N$ expansion in a generalised model with N valleys (particle flavours) between which disorder can scatter. SCBA results thus become exact in the limit $N \rightarrow \infty$.

For states with $E = 0$, Eq. (2) has only the trivial $\Gamma = 0$ solution for disorder strength weaker than the critical value

$$\varkappa_c^{SCBA} = \left[\int_{|\mathbf{k}| < K_0} \frac{d^d \mathbf{k}}{(2\pi)^d} \frac{1}{a^2 k^{2\alpha}} \right]^{-1}, \quad (4)$$

while for $\varkappa > \varkappa_c$ there is a nontrivial $\Gamma \neq 0$ solution, where K_0 is the ultraviolet momentum cutoff set by the bandwidth or the inverse impurity size r_0^{-1} . Thus, the SCBA predicts a disorder-driven phase transition at the critical disorder strength \varkappa_c , Eq. (4) (provided it is non-zero) between phases with $\Gamma = 0$ and $\Gamma \neq 0$.

In the case of low dimensions, $d < 2\alpha$, $\varkappa_c^{SCBA} = 0$, suggesting a finite scattering rate for all disorder strengths and the absence of the phase transition. For high dimensions ($d > 2\alpha$), the critical disorder strength \varkappa_c^{SCBA} is non-zero, signalling a possible phase transition.

The SCBA and the (equivalent in the leading order) large- N approach have also been used to analyse disorder-driven criticality for 3D Dirac fermions in Refs. (18) and (19). In

Ref. (22) the SCBA was used to compute the conductivity near the non-Anderson disorder-driven transition in a Weyl semimetal.

Criticism of the SCBA. While the SCBA is justified in the limit of an infinite number of valleys, $N \rightarrow \infty$, it becomes inaccurate for realistic materials with finite N . The SCBA has been criticised in the context of graphene in Ref. (60) and also later discussed in detail in Ref. (61). Although graphene corresponds to the marginal dimension $d = 2\alpha$ and does not exhibit a transition, the criticism of Refs. (60) and (61) also applies to all systems in higher dimensions $d \geq 2\alpha$ [a detailed analysis of the SCBA for higher-dimensional systems and Weyl semimetals may be found in Refs. (23) and (25) respectively].

When applied to realistic systems, the SCBA takes into account certain contributions to physical observables, e.g. the density of states and conductivity, and systematically neglects other contributions of the same order of magnitude(60, 61, 23, 25). Thus, controlled methods, to which we turn in the next section, are necessary to analyse more systematically the nature of the disorder-driven transition.

2.3. Renormalisation-group analysis

Non-Anderson disorder-driven transitions can also be analysed using a more systematic renormalisation group (RG) approach(62, 63, 64), which is controlled by the small parameter $\varepsilon = 2\alpha - d$ (23). The celebrated approach consists in coarse-graining the system by integrating out the high-momentum degrees of freedom down to an ultraviolet momentum cutoff $K = K_0 e^{-l}$, thereby renormalising the system properties at lower momenta, where K_0 is set by the bandwidth or disorder correlation length. For simple potential disorder, which is the most common in realistic systems, the associated RG flow of the dimensionless disorder strength, $\gamma(l) \propto \varkappa K^{-\varepsilon}$, is given by

$$\partial_l \gamma = (2\alpha - d)\gamma + \gamma^2 + \dots \quad (5)$$

We note that the dimensionless disorder strength γ is of the order of the inverse Ioffe-Regel parameter(24) $(k\ell)^{-1}$, which plays an important role in the theory of transport and localisation in disordered systems(3, 4, 5). The first term in the right-hand side of Eq. (5) arises from the power-counting for the random perturbation at the Gaussian disorder-free fixed point. The second term, quadratic-in-disorder, arises from the one-loop corrections to the strength of disorder corresponding to the diagrams in Fig 3.

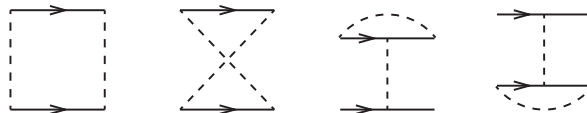


Figure 3

Diagrams for the one-loop renormalisation of the disordered strength.

In accordance with the arguments of Sec. 2.1, Eq. (5) shows that weak disorder strength always grows at low momenta in low dimensions ($d < 2\alpha$). However, slightly above the marginal dimension, $d_c = 2\alpha$, i.e. for small negative values of $\varepsilon = 2\alpha - d$, the disorder strength flows to larger or smaller values, depending on whether or not it exceeds the critical value $\gamma_c = |\varepsilon|$. This signals the aforementioned disorder-driven quantum phase transition.

Some realistic systems, such as arrays of (optically or magnetically) trapped ions(45, 46, 49, 47, 48) can be tuned(44) to realise arbitrarily small values of ε . Other systems, such as semiconductors or Weyl semimetals, can realise only integer values of α and d , leading to integer values of ε of order unity.

Although the above RG analysis is controlled quantitatively only for small ε , we expect that the phase transition and its qualitative properties persist to values of ε of order 1, assuming the absence of a phase transition as a function of ε (which, strictly speaking, cannot be excluded). Indeed, the numerical results for the DoS in Weyl (Dirac) semimetals(21, 29, 30, 27, 32) and in chains of trapped ions(44) agree well with the one-loop RG analysis for $|\varepsilon| \sim 1$, as we will discuss in more detail in Sec. 3.

An RG approach of this type was developed nearly three decades ago(65) to describe 2D Dirac fermions in the context of the Ising model. Later it was applied to 2D Dirac quasiparticles in integer-quantum-Hall systems(66) and d -wave superconductors(67, 68) [see also Ref. (69)]. More recently, a comprehensive RG description for electrons in graphene with various disorder symmetries has been developed in Ref. (60) and further discussed in Ref. (61). Although 2D Dirac quasiparticles experience renormalisation effects from elastic scattering through all momentum states corresponding to the linear dispersion, they correspond to the critical dimension $d = 2\alpha = 2$ ($\varepsilon = 0$) and do not exhibit the transition.

A non-Anderson disorder-driven transition was first studied in this type of RG framework for 3D fermions ($\alpha = 1$, $d = 3$) in Ref. (20), also taking into account the electron-electron interaction. Such approaches are now being used very broadly to study the properties of the transition and critical behaviour of physical observables in Weyl semimetals [see, e.g., Refs. (23, 24, 26, 27, 32, 33, 35, 36, 37, 38)], where again $\alpha = 1$ and $d = 3$. In Refs. (23) and (24) it was demonstrated that such non-Anderson transitions are not specific to Dirac and Weyl systems, but exist in all systems in high dimensions, $d > 2\alpha$, as can be seen when the RG analysis is applied to generic semiconductor-like and high-dimensional chiral systems. In particular, in Ref. (44) this RG analysis was applied to 1D spin chains mapped onto the problem of a single particle with a power-law dispersion in a random potential, leading to the prediction of the unconventional disorder-driven phase transition in such systems.

2.4. Non-Anderson vs. Anderson transitions

We emphasise that the disorder-driven transition discussed in the previous subsections is distinct from the conventional Anderson metal-insulator transition. While the former manifests itself in physical observables only near nodes and band edges, the usual Anderson localisation occurs for all states away nodes and band edges (and is usually observable in the conductivity, which is determined by the states at the Fermi level).

In the presence of a finite Fermi surface, one may introduce, in the spirit of the Fermi-liquid theory(3, 4, 5), effective (measurable in experiment) constant DoS, electron mass and elastic scattering time near the Fermi surface. It is usually assumed that scattering processes through momenta far from the Fermi surface (see Fig. 4) can be absorbed in these effective parameters of the low-energy quasiparticles. The single-particle physics is then described by the non-linear sigma-model(5) in terms of diffusive electron modes on distances larger than the mean free path ℓ . This model is believed to exhibit only one disorder-driven transition, namely the Anderson localisation transition. The critical properties of the Anderson transition are believed to be universal, depending only on the dimensionality

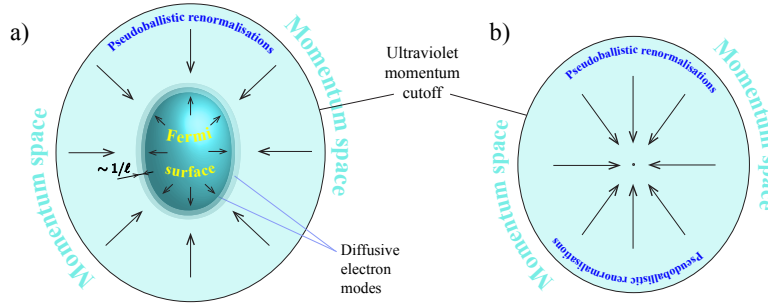


Figure 4

Pseudoballistic (on scales shorter than the mean free path ℓ) renormalisation in high-dimensional ($d > 2\alpha$) systems. a) For electrons at the Fermi energy, the RG is cut off by the Fermi surface. The resulting renormalised parameters are an input for describing diffusive electron modes in the momentum shell of the width $\sim 1/\ell$ near the Fermi surface. b) For electrons near a band edge or a node, the pseudoballistic RG flow persists to the lowest momenta. The effective ultraviolet momentum cutoff is determined by the correlation length of the random potential or the band width in momentum space.

of space, underlying symmetry class, and topology, but independent of the microscopic details. In particular, in dimensions $d = 2 + \varepsilon$, the Anderson criticality can be described analytically(70, 5) using an RG approach, controlled by the small parameter $\varepsilon > 0$, in the framework of the non-linear sigma-model. The renormalisations considered in Sec. 2.3 determine system properties on length scales shorter than the mean free path ℓ (24) and may be termed “pseudoballistic”. These renormalisations are cut off by the Fermi momentum, so long as $k_F \ell(k_F) \gtrsim 1$, and thus determine only the input parameters of the sigma-model, but do not affect the Anderson criticality.

However, as we have seen above, the phenomenology is very different near nodes and band edges, where the quasiparticle parameters (density of states, scattering rate, etc.) can vanish or demonstrate non-analytic behaviour due to the renormalisation by high-momentum modes, leading to the failure of the conventional sigma-model description. As a consequence, one may expect non-Anderson disorder-driven transitions near nodes and band edges. As we discussed in the previous subsections, such unconventional transitions are indeed found in systems in high dimensions.

2.5. Related phenomena in disorder-free interacting systems

The effective action, describing a single particle with energy E and dispersion $\epsilon_{\mathbf{k}} = ak^\alpha$ in a random short-range-correlated potential, in the supersymmetric(5) and replica(71) representations is given by

$$\mathcal{L} = -i \int_{\mathbf{r}} \bar{\psi} (E - \epsilon_{\mathbf{k}} + i0 \cdot \Lambda) \psi + \frac{1}{2} \varkappa \int_{\mathbf{r}} (\bar{\psi} \psi)^2, \quad (6)$$

with $\bar{\psi}$ and ψ being supervectors(5) or vectors with components in replica space(71), respectively. A similar action can also be written in Keldysh representation(72). As the action (6) resembles that of the ϕ^4 theory, the critical behaviour at the non-Anderson disorder-driven transition resembles that of a number of disorder-free interacting systems.

A prominent example here is the field theory of a self-avoiding polymer in d dimensions(73) with interaction strength g . The RG flow of the coupling g is also given by Eq. (5) with $\gamma \rightarrow -g$ and $\alpha = 2$. The fixed point characterising the anomalous long-scale properties of a self-avoiding polymer appears in $d < 4$ dimensions.

Phase transitions driven by high momenta or energies are known to occur also in dilute weakly interacting (74, 75, 76) and Feshbach-resonant Bose gases(77, 78, 79), as well as in fermionic gases near unitarity(80, 81, 82) (BCS-BEC crossover). Similar renormalisations of low-energy quasiparticle properties due to scattering through high-energy states occur in strongly disordered bosonic insulators(83, 84), with a similar critical point for the DoS increasing at low energies.

3. PHYSICAL OBSERVABLES NEAR THE TRANSITION

3.1. Critical exponents

Under the assumption of single-parameter scaling, a continuous phase transition is characterised by a single divergent correlation length, $\xi \propto |\varkappa - \varkappa_c|^{-\nu}$, at the critical energy $E = E_c$, with a universal correlation-length exponent ν , and the characteristic energy $|E - E_c| = E^* \propto \xi^{-z}$, where z is the universal dynamical exponent. The scale $E^*(\varkappa) \propto (\varkappa - \varkappa_c)^{z\nu}$ serves as a crossover energy between several distinct types of behaviour of conductivity, DoS, and other physical observables, as illustrated in Fig. 2. When Anderson localisation is allowed by symmetry in a high-dimensional system, we expect the scale E^* to determine the position of the mobility threshold for $\varkappa > \varkappa_c$. The critical exponents can be observed experimentally, for example, through the critical behaviour of the DoS and conductivity, as we discuss in Secs. 3.2 and 3.4 below.

The correlation-length exponent $\nu = 1/(d - 2)$ for d -dimensional Weyl fermions has been computed in the SCBA ($N = \infty$ approach) in Ref. (6) and has also been evaluated at next-to-leading order in $1/N$, together with the dynamical exponent z , in Ref. (19). For 3D Dirac and Weyl semimetals, the one-loop RG analysis predicts $\nu = 1$, $z = 3/2$, result first obtained in Ref. (20). Near the band edge of a semiconductor the one-loop critical exponents are given by $\nu = (d - 2\alpha)^{-1}$ and $z = \alpha/2 + d/4$ for arbitrary α and d (24).

Field theories of Weyl particles in a random potential [in replica(71), supersymmetric(5), or Keldysh(72) formulations] can be mapped onto the Gross-Neveu model(85) in the limit of a vanishing number of fermion flavours, $N \rightarrow 0$, and with the opposite (attractive) sign of the coupling. The critical properties of the Gross-Neveu and equivalent models have been studied extensively in the literature [see, e.g., Refs. (86, 87, 88, 89, 90, 91, 92, 93, 94)], with the critical exponents known up to fourth-loop order. A similar two-loop RG analysis for graphene have been carried out in Ref. (95). Critical exponents for Weyl particles in $2 + \varepsilon$ dimensions have been evaluated explicitly to two-loop order in Ref. (33).

Critical exponents for 3D Weyl and Dirac systems have been obtained numerically, using the critical scaling of the DoS in Refs. (21, 26, 27, 29, 32) and using conductance scaling in Ref. (30); some of the results are shown in Table 1 and demonstrate that the dynamical exponent is very close to the one-loop RG result $z = 3/2$, while the correlation-length exponent may significantly deviate from the one-loop prediction $\nu = 1$.

Ref.	(30)	(21)	(29)	(39)	(32)
System	Single-node WSM	DSM	WSM	WSM	WSM
ν	1.47 ± 0.03	1.00 ± 0.15	0.84 ± 0.1	1.01 ± 0.06	$0.72 \pm 0.2 - 1.1 \pm 0.15$
z	1.49 ± 0.02	1.5 ± 0.1	1.53 ± 0.03	$z = 1.50 \pm 0.04$	$1.38 - 1.49 \pm 0.05$

Table 1 Numerical values of the correlation-length (ν) and dynamical (z) exponents for 3D Weyl and Dirac systems.

3.2. Density of states

The existence of the critical point together with the assumption of the single-parameter scaling suggests that the DoS near the critical point has the scaling form(21)

$$\rho(E, \varkappa) = (E - E_c)^{\frac{d}{z}-1} \Phi \left[(\varkappa - \varkappa_c) / (E - E_c)^{\frac{1}{z\nu}} \right] + \rho_{\text{smooth}}, \quad (7)$$

where Φ is an arbitrary function (that may be different for $E < E_c$ and $E > E_c$). Here ρ_{smooth} is a smooth analytic contribution, which is generically allowed by the scaling theory and has been demonstrated microscopically to exist in models with smooth disorder(40, 41, 42, 43, 24). The form (7) of the critical DoS was first proposed (without the smooth contribution) and verified numerically for 3D Dirac particles in Ref. (21).

Depending on the range of the disorder strength \varkappa and energy E , a high-dimensional system may exhibit several qualitatively different types of the DoS behaviour, shown in Fig. 2, which were first discussed for 3D Dirac systems in Ref. (21). Near the critical disorder strength, $\varkappa \approx \varkappa_c$, at the ‘‘critical regions’’ in Fig. 2, the DoS behaves as $\rho \propto |E - E_c|^{\frac{d}{z}-1} + \rho_{\text{smooth}}$. For strong disorder, $\varkappa > \varkappa_c$, the DoS is constant at low energies, $\rho \propto (\varkappa - \varkappa_c)^{(d-z)\nu} + \rho_{\text{smooth}}$. For subcritical disorder, $\varkappa < \varkappa_c$, the DoS has the same energy dependence as in a disorder-free system, $\rho \propto (\varkappa_c - \varkappa)^{-d\nu(\frac{z}{\alpha}-1)} E^{\frac{d-\alpha}{\alpha}} + \rho_{\text{smooth}}$, with the effects of disorder reflected in a prefactor that diverges at the critical point. The scaling form (7) of the DoS near nodes and band edges in semiconductors and semimetals is supported by rigorous microscopic calculations (24). The DoS in a 3D Dirac semimetal as a function of energy E for various disorder strengths(21) is shown in Fig. 5.

We note that the analytic contribution ρ_{smooth} is normally rather small and has remained undetectable in all numerical studies(21, 25, 44, 26, 27, 29, 30, 31, 32) so far, other than Refs. (34) and (39). This contribution is determined by the rare-region effects discussed in Sec. 5. It has also been suggested [see, e.g., Refs. (34) and (39)] that such effects might smear the criticality in a small region close to the transition, converting it into a sharp crossover. However, in most of this review we do not distinguish between such a crossover and a real transition; more details on this topic are presented in Sec. 5.

3.3. Mobility threshold

In a disordered system, localised and delocalised states do not coexist at the same energy(96), which allows one to introduce the concept of mobility threshold, the energy separating localised and delocalised states(97).

The high-dimensional disorder-driven transition manifests itself in the unusual behaviour of the mobility threshold as a function of disorder strength(24), provided the existence of both localised and delocalised states is allowed by dimensions, symmetry, and topology, as in the case of $d > 2$ -dimensional semiconductors in the orthogonal symmetry class.

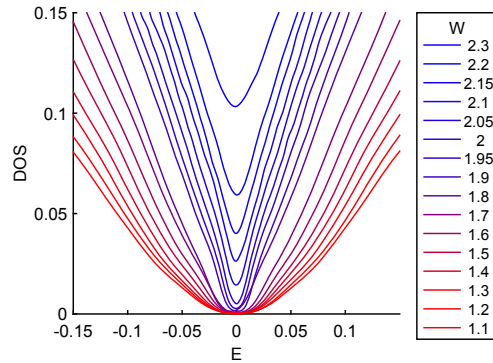


Figure 5

[Adapted from Ref. (29)] Critical behaviour of the density of states near the non-Anderson transition in a Weyl semimetal as a function of energy for various random amplitudes W ($\sim \kappa^{\frac{1}{2}} r_0^{-\frac{d}{2}}$). The DoS near the node is strongly suppressed and can be approximated as $\rho \propto E^2$ if the disorder strength is smaller than a critical value(29), $W < W_c \approx 2$. For $W > W_c$ the zero-energy density of states grows rapidly with the disorder amplitude W .

For weak disorder, $\kappa < \kappa_c$ the mobility threshold is pinned to the band edge due to the smallness of the renormalised disorder strength. For supercritical disorder, however, the effective disorder strength increases near the band edge, until it reaches the strong-coupling point, $\gamma \sim 1$, resulting in the localisation of all states in a trivial-topology system in the orthogonal symmetry class for $\gamma \lesssim d - 2$ (5). Just above two dimensions this leads to the non-analytical behaviour of the mobility threshold(24) illustrated in Fig. 2a, which can be expected to hold in all high dimensions $d > \max(2\alpha, 2)$. This non-analytic behaviour of the mobility threshold should be contrasted with the case of low dimensions $d < 2\alpha$, where the mobility threshold is a smooth function of the disorder strength(98, 5, 56).

We note that for non-trivial topology and various disorder symmetries the phase diagram of a high-dimensional disordered system can be more complicated. For example, it has been shown recently(26) that the states near the nodes of a 3D Dirac system with axial and potential disorder experience two distinct transitions when disordered strength is increased: the high-dimensional non-Anderson transition and, at larger disorder, the conventional Anderson transition. The behaviour of the mobility threshold and its interplay with the non-Anderson disorder-driven transition for Dirac (Weyl) systems can be studied rigorously analytically in $d = 2 + \varepsilon$ dimensions but currently remains a future research direction.

3.4. Conductivity

The unconventional disorder-driven transition can be studied through the conductivity of a system, which is a quantity readily measured in condensed-matter experiments. We note that in $d \leq 2$ -dimensional systems in the orthogonal class with trivial topology, such as arrays of trapped ions(45, 46, 49, 47, 48), all excitations are localised, resulting in a vanishing conductivity, $\sigma = 0$. By contrast, some systems, such as chiral 1D chains(44), may lack backscattering, in which case the conductivity is always nonzero.

Single-parameter scaling suggests a generic form of the conductivity(23) (the response

of the current of particles at energy E to an electric field),

$$\begin{aligned}\sigma(E, \varkappa) &\sim \xi^{-(d-2)} G[(E - E_c)\xi^z] \\ &= |\varkappa - \varkappa_c|^{\nu(d-2)} G[(E - E_c)/|\varkappa - \varkappa_c|^{z\nu}],\end{aligned}\quad (8)$$

where the scaling function G is in general different for subcritical and supercritical disorder.

It follows from Eq. (8) that the conductivity at the node of a semimetal at zero temperature $T = 0$ behaves as $\sigma \propto |\varkappa - \varkappa_c|^{\nu(d-2)}$ (23). We note that the conductivity can be nonzero or vanish on the strong-disorder side $\varkappa > \varkappa_c$, depending on the existence and the behaviour of the mobility threshold. Equation (8) also suggests that in a disordered semimetal with the chemical potential at the nodal point, the conductivity at the critical disorder strength ($\varkappa = \varkappa_c$) exhibits the universal temperature dependence $\sigma \propto T^{(d-2)/z}$ (23).

Conductivity of a Weyl semimetal The conductivity near the unconventional disorder-driven transition has received particular attention in the context of WSMs, which are currently the most experimentally available system in high dimensions ($d > 2\alpha$).

A remarkable feature of WSMs is the absence of localisation by smooth disorder that does not scatter between different Weyl nodes. Because a single-node WSM is the surface of a 4D topological insulator, it is topologically protected from localisation(99, 12). We note that realistic materials always have an even number of Weyl nodes, according to the fermion doubling theorem(100). However, for sufficiently smooth disorder internodal scattering can be neglected (e.g., if the length of internodal scattering exceeds the dephasing or magnetic length), and the material behaves as an even number of independent copies of a single-node WSM. The conductivity in such system is finite at all disorder strengths, with the possible exception of the critical point.

For weak disorder, $\varkappa \ll \varkappa_c$, the conductivity of a single-node WSM can be computed, e.g., using the kinetic equation(22) or diagrammatically(23, 101), with the result

$$\sigma = \frac{e^2 v^2}{2\pi \varkappa}.\quad (9)$$

Expressions similar to Eq. (9), but with different prefactors, have been obtained also in Refs. (102) and (103) neglecting the renormalisation of the velocity vertex by disorder.

Perturbative calculations(22, 23, 101, 102, 103) of the conductivity, Eq. (9), valid for $\varkappa \ll \varkappa_c$, neglect the pseudoballistic renormalisation of the system properties, which can be taken into account by means of the RG described in Section 2.3, with the infrared momentum cutoff determined by E_F in an infinite system at zero temperature. This approach is valid below the transition, $\varkappa < \varkappa_c$ (when disorder is irrelevant), but is limited to high Fermi energies above the transition, $\varkappa > \varkappa_c$ [when disorder is relevant but must remain weak ($k_F \ell(k_F) \gg 1$)]. The conductivity is given(23) by Eq. (9) with the “bare” disorder strength \varkappa replaced by its renormalised value $\tilde{\varkappa}(E_F)$ [for the SCBA analysis of the conductivity see also Ref. (22)].

For strong disorder, $\varkappa > \varkappa_c$, the conductivity has also been obtained using order-of-magnitude estimates and the scaling theory in Ref. (23). An effective field theory for WSMs at strong disorder has been developed in Refs. (104) and (105). The conductivity of a single-node WSM as a function of the disorder strength \varkappa and temperature T is shown in Fig. 6.

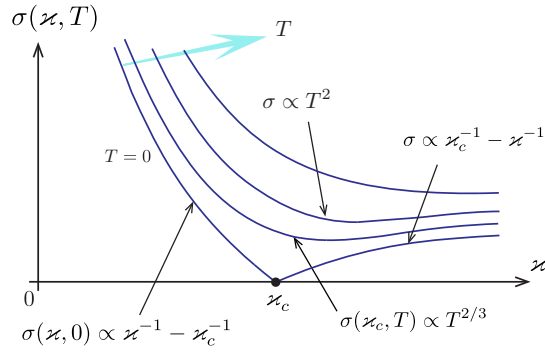


Figure 6

[Adapted from Ref. (23)] Conductivity of a single-node WSM as a function of disorder strength for various temperatures. The exponents for the dependencies on disorder strength and temperature near the transition are obtained within perturbative one-loop RG treatment.

Transport in WSMs has been studied numerically in Refs. (25) and (106), utilising a smooth random potential with a long correlation length resulting in suppressed internodal scattering. References (25) and (106) reported a vanishing conductivity for subcritical disorder $\kappa < \kappa_c$ and a finite conductivity for supercritical disorder $\kappa > \kappa_c$. Such a behaviour seemingly contradicts Eq. (9), the result of rigorous analytical calculations(22, 23, 101, 102, 103), which gives a nonzero conductivity for $\kappa \ll \kappa_c$. As noted in Ref. (25), this discrepancy is explained by the noncommutativity of the limits $E_F = 0, L \rightarrow \infty$ and $E_F \rightarrow 0, L = \infty$, where the Fermi energy E_F is measured from the Weyl node and L is the system size. Numerical simulations(25, 106) carried out for finite samples and zero chemical potentials yield zero weak-disorder conductivity (extracted respectively from the conductance), while analytical calculations(22, 23, 101, 102, 103) deal with the limit of an infinite sample and the chemical potential sent to zero at the end of the calculation, which results in a finite conductivity. This non-commutativity is explained by finite-size effects(25, 23) discussed in detail in Sec. 4.

We emphasise that the calculations (22, 23, 101, 102, 103, 104) of the conductivity in a WSM, discussed in this section, are based on the assumption that the disorder potential may be considered short-range [cf. Eq. (2)] for scattering processes within one node. By contrast, in solid-state WSMs disorder is dominated normally by Coulomb impurities, leading to long-range random potential. The presence of charged impurities may result in a finite conductivity for all disorder strengths(43), as discussed in Sec. 6.1.1 below.

3.5. Multifractality

Wavefunction multifractality (fractal structure characterised by an infinite set of exponents) has been a subject of extensive studies in the context of Anderson and quantum Hall transitions [see Refs. (5, 107) for review] and is characterised by the inverse participation ratios(108) (IPRs) $P_q = \int |\psi(\mathbf{r})|^{2q} d\mathbf{r}$. These quantities describe how extended the wavefunction $\psi(\mathbf{r})$ is and have two obvious limits: for delocalised states that uniformly fill the whole system $P_q \propto L^{-d(q-1)}$, while for localised states the IPRs are system-size-independent, $P_q = \text{const.}$ For multifractal wavefunctions disorder-averaged IPRs behave as

$P_q \propto L^{-d(q-1)-\Delta_q}$ with a non-linear (as a function of q) multifractal spectrum Δ_q (where $\Delta_q = 0$ corresponds to the extended plane-wave-like states $\psi \propto L^{-\frac{d}{2}}$).

It has been shown recently that the high-dimensional disorder-driven transition also exhibits wavefunction multifractality (regardless of whether the system allows for a localisation transition), with the spectrum different from that of the Anderson transition. Within an $\varepsilon = d - 2\alpha$ -expansion the multifractal spectrum is given by(37)

$$\Delta_q = \frac{1}{2}(2\alpha - d)q(q - 1) + \mathcal{O}[(d - 2\alpha)^2] \quad (10)$$

for a semiconductor in the orthogonal symmetry class and

$$\Delta_q = -\frac{3}{8}(d - 2)^2 q(q - 1) + \mathcal{O}[(d - 2)^3] \quad (11)$$

for Weyl particles in d dimensions. The multifractal spectrum (11) matches that of 2D Dirac fermions (with ε replaced by the dimensionless disorder strength), as studied in Ref. (109). We note that for 2D Dirac fermions there is no phase transition, although on sufficiently short length scales the wavefunctions display *non-universal* fractal behaviour(109, 110). By contrast, the multifractal behaviour described by Eqs. (10) and (11) persists on all length scales at non-Anderson disorder-driven transitions. As a result of multifractality, moments of physical observables (e.g. conductance or DoS) may be expected to have infinite sets of critical exponents at the transition point. Also, different scaling behaviour of typical and average DoS, observed recently in a Dirac semimetal in Ref. (26), has been argued to be a reflection of the wavefunction fractality(26).

4. FINITE-SIZE EFFECTS IN HIGH DIMENSIONS

Finite-size effects in high dimension $d > 2\alpha$ are qualitatively different from the case of low dimensions and lead to several qualitatively new phenomena.

4.1. Level discreteness and ballistic transport in disordered systems

A finite disorder-free system is characterised by a discrete spectrum of energy levels, E_n , as a result of spatial quantisation. In the presence of disorder, the levels get broadened, which results in a smooth disorder-averaged DoS $\rho(E)$ as a function of energy if the elastic scattering rate $\tau^{-1}(E)$ exceeds the level spacing $|E_n - E_{n-1}|$. In a conventional (low-dimensional, $d < 2\alpha$) system the disorder-averaged DoS $\rho(E)$ in the presence of arbitrarily weak disorder is a smooth function for all energies E , which are allowed by the bandwidth and disorder amplitude, in the limit of infinite system size.

A contrasting remarkable feature of high-dimensional ($d > 2\alpha$) systems is that the levels near nodes and band edges remain discrete(37), with a sharply peaked DoS $\rho(E)$ (see Fig. 7), for disorder $\varkappa < \varkappa_c$, irrespective of how large the system is (and provided rare-region effects discussed in Sec. 5 are neglected). Specifically, the level spacing $|E_n - E_{n+1}|$ for energy levels closest to the node or a band edge exceeds the ‘‘level width’’ given by the elastic scattering rate(37, 23). This is a reflection of the elastic scattering rate $\tau^{-1}(E) \sim \gamma(E)(E - E_c)$ decreasing faster than the energy $E - E_c$ when approaching a node or a band edge, as discussed above.

When the system size is increased, the spacing between all levels decreases, but the level width of the lowest-energy levels decreases faster than the spacing, so that the lowest levels

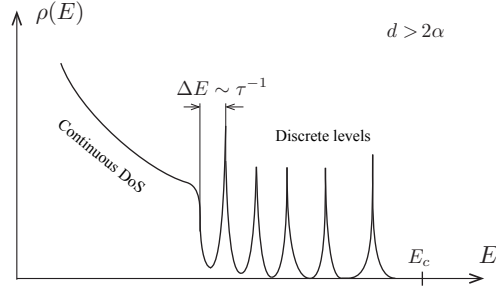


Figure 7

The density of states near a band edge in a high-dimensional ($d > 2\alpha$) system. At low energies the DoS necessarily exhibits level discreteness, which is a reflection of the irrelevance of subcritical disorder.

always remain discrete. For a system with the small parameter $|\varepsilon| = |d - 2\alpha| \ll 1$, there are $N_\varepsilon \sim 1/|\varepsilon|$ of discrete levels (sharp peaks of the DoS) at the critical disorder $\varkappa = \varkappa_c$, while the rest of the spectrum is smooth(37).

Moreover, for the discrete levels the elastic scattering time τ exceeds the ballistic Thouless time $\tau_{\text{Th}} = L/v$ required for a particle to propagate through the system. The transport of quasiparticles sufficiently close to band edges and nodes is therefore always ballistic in arbitrarily large high-dimensional systems for $\varkappa < \varkappa_c$.

4.2. Conductance of finite semimetallic samples

The level discreteness discussed above is reflected in the conductance of a finite semimetallic sample in high dimensions if the Fermi energy E_F (measured from the node) and the temperature are smaller than the level spacing near the node(23). Indeed, the transverse momentum is quantised in a finite sample between two reservoirs (Fig. 8a). Depending on the boundary conditions in the transverse direction, a small Fermi energy E_F either lies below the minimal excitation energy or corresponds to only one transverse mode. The conductance of such a system, therefore, does not exceed the spin and valley degeneracy of one transverse mode, $G \lesssim g$, according to the Landauer formula.

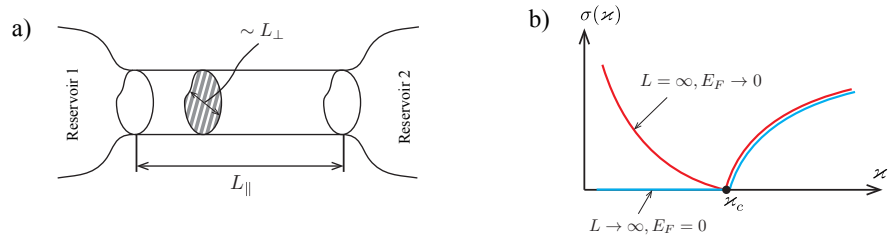


Figure 8

a) Set-up for measuring the conductance of a finite sample. b) Conductivity of a single-node Weyl semimetal in the limits of an infinite sample and small finite Fermi energy ($L = \infty, E_F \rightarrow 0$) and of a large finite sample and zero Fermi energy ($L \rightarrow \infty, E_F = 0$). The two limits do not commute for subcritical disorder, $\varkappa < \varkappa_c$ (25, 23).

Therefore, the conductivity of a finite semimetallic sample, defined as $\sigma = G \frac{L_{\parallel}}{S_{\perp}} \lesssim \frac{g L_{\parallel}}{L_{\perp}^2}$, vanishes in the limit of infinite system size, $L_{\parallel} \propto L_{\perp} \rightarrow \infty$, where L_{\perp} and L_{\parallel} are the transverse and longitudinal sizes of the sample, as shown in Fig. 8a. Vanishing conductivity for $\varkappa < \varkappa_c$ and Fermi level located at the node ($E_F = 0$) has been reported in numerical simulations of transport in finite-size WSM systems in Refs. (25) and (106), in accordance with the above argument.

In contrast, analytical calculations of conductivity(22, 23, 101, 102, 103), discussed in Sec. 3.4 and based on the kinetic equation and the Kubo formula, deal with the limit of an infinite sample, $L_{\parallel} = L_{\perp} = \infty$, and a finite chemical potential (that may be taken to zero at the end of the calculation), leading to a nonzero conductivity of a WSM for subcritical disorder, $\varkappa < \varkappa_c$.

The behaviour of the conductivity as a function of disorder strength is shown in both limits in Fig. 8b. As noted in Ref. (25), each limit can be effectively realised in experiment. Finite conductivity (the infinite-sample regime) can be expected if the temperature or the rate of inelastic scattering exceed the level spacing near the node. Otherwise, the limit of a finite system and zero Fermi energy is realised, giving zero conductivity for subcritical disorder strengths.

We note that, in addition to the bulk states discussed above, a material can host surface states that also contribute to conductance. One important example is the contribution of the surface states of a WSM(12) to the conductance, which can be estimated as(29) $G_{\text{surf}} \sim L_{\perp} K_0$, with K_0 being the separation between the Weyl nodes in momentum space. This surface component significantly exceeds the bulk contribution to the conductance of an undoped WSM at low temperatures.

5. RARE-REGION EFFECTS

Perturbative RG and SCBA analyses in high-dimensional systems suggest that the DoS vanishes at nodes and band edges for subcritical disorder and has a finite value otherwise. Thus, the RG and SCBA approaches suggest that the DoS at nodes and band edges can serve as an order parameter for the unconventional disorder-driven transition.

However, it has been known for three decades(40) that disorder with a smooth distribution function always leads to a non-vanishing disorder-averaged density of states at all energies allowed by the band width and the amplitude of the random potential. Strictly speaking, nodes (points with zero DoS away from band edges) do not exist in disordered systems, and band edges exist only for bounded (having finite maximal amplitude) disorder. Concomitantly, this well-known result demonstrated that the DoS is not an order parameter that can distinguish between low- and high-disorder phases [as was emphasised recently for Weyl semimetals in Ref. (42)].

This broadening of nodes and the appearance of states far below the band edges in disorder-free samples occurs as a result of statistically rare non-perturbative fluctuations of the disorder potential, that is unaccounted for by the perturbative RG.

We emphasise, however, that the DoS not being an order parameter (or even the absence of any order parameter) does not preclude the existence of a genuine sharp transition manifested, for example, in non-analytic behaviour of physical observables across the critical point (as exemplified by Kosterlitz-Thouless transition).

5.1. Lifshitz tails

Rare fluctuations of the disorder potential lead to the existence of arbitrarily deep potential wells that trap particle states (provided the existence of localised states is allowed by symmetry and/or topology), leading to the formation of “Lifshitz tails”, states with energies significantly below the band edge of a disorder-free system, as shown in Fig. 2. Lifshitz tails have been studied extensively (111, 112, 113, 114) for conventional low-dimensional ($d < 2\alpha$) semiconductors. The DoS ρ_{tail} in Lifshitz tails is non-universal and depends strongly on the microscopic details of disorder. For Gaussian disorder and quadratic quasiparticle dispersion, $\rho_{\text{tail}}(E) \propto \exp(-c|E|^{2-d/2})$ for sufficiently low energies E and $d < 4$, with c being a constant. In the field-theoretical representation [cf. action (6)] the rare-region effects correspond to instantons [see Ref. (115) for review], which cannot be taken into account at any order in perturbation theory.

In high dimensions, the form of Lifshitz tails is qualitatively different from the case of low-dimensions. It has been shown in Ref. (41), by analysing instantonic contributions to the replica field theory, that for $d > 4$ and quadratic dispersion, the DoS in the presence of Gaussian disorder of strength \varkappa behaves according to

$$\rho_{\text{tail}}(E) \propto e^{-c_1(c_2+|E|)^2/\varkappa}, \quad (12)$$

where c_1 and c_2 are \varkappa -independent constants and the disorder correlation length is assumed fixed. In Ref. (24) it was shown that the dependency (12) of the DoS in Lifshitz tails on energy and disorder strength persists generically for systems with the dispersion $\epsilon_{\mathbf{k}} \propto k^\alpha$ in any dimension $d > 2\alpha$.

We note that in semimetals that allow for localisation the smearing of nodes can be also effectively viewed as the beginning of Lifshitz tails. However, in semimetals that are topologically protected from localisation the smearing of nodes requires a separate analysis. In particular, a detailed microscopic analysis of the DoS for a single-node Weyl semimetal has been carried out recently in Ref. (42). It has been demonstrated that the DoS at the node is finite and exponentially small in disorder strength.

In systems just above the critical dimension ($1 \gg d - 2\alpha > 0$), the DoS in the Lifshitz tail is strongly suppressed at all energies, with $\rho_{\text{tail}}(0) \propto e^{-\frac{1}{d-2\alpha} \frac{\varkappa_c}{\varkappa}}$ (24), which near the transition ($\varkappa \lesssim \varkappa_c$) allows one to separate accurately the band states (“weak-disorder” phase in Fig. 2) from the tail. This contrasts with the case of low dimensions ($d < 2\alpha$), where the beginning of the Lifshitz tail is not parametrically suppressed. One may show that a large number of valleys N also leads to the suppression of the rare-region contribution to the DoS, with $\rho_{\text{tail}}(0) \propto e^{-N \frac{\varkappa_c}{\varkappa}}$. Thus, the contributions of the rare-region effects to the density of states are suppressed when the system properties are computed in large- N and small- ε -controlled RG approaches. This allows one to use the DoS as an effective order parameter for the unconventional disorder-driven transition so long as the exponentially small rare-region contribution is neglected.

Realistic 3D Dirac and Weyl semimetals ($\alpha = 1$, $d = 3$), the best known and most extensively studied class of systems for the high-dimensional phenomena discussed in this review, have neither a small parameter ε nor a large number of valleys N . Nevertheless, the contributions of rare-region effects to physical observables in these systems appear to be rather small and have been undetectable in most numerical studies of the DoS and transport (21, 25, 26, 27, 29, 30, 31, 32) to date, with the exception of the recent simulations (34, 39). Because such systems have no small parameters at the critical point, the reason

for the suppression of rare-region effects in 3D Weyl (Dirac) systems, observed numerically, currently remains to be investigated.

5.2. Phase transition vs. sharp crossover

Another potential consequence of rare-region effects, currently not demonstrated analytically, is a possible broadening of the quantum critical region, which may convert the transition into a sharp crossover. So far we have not distinguished between these two scenarios and we have used the term “non-Anderson disorder-driven transition” to label either a true transition or a sharp crossover.

The elimination of the transition has been advocated recently in the numerical studies of 3D Dirac semimetals in Refs. (34) and (39), which suggest smooth and analytic behaviour of the disorder-averaged DoS, which in turn was additionally averaged with respect to the boundary conditions in a finite sample.

We note that the phenomenology of rare-region effects and their interplay with perturbative effects are qualitatively distinct in systems where Anderson localisation is allowed by symmetry and topology and systems where localisation is forbidden. While in the conventional analyses(111, 112, 113, 114, 41) rare-region effects come from localised states, their nature should be different in materials like single-node WSMs and 1D chiral chains(44), where states are topologically delocalised, and thus deserve a separate study.

While in a WSM power-law-localised (bound) states $\psi \sim 1/r^2$ exist in a single potential well(42), in a random potential such states (decaying slower than $1/r^d$) inevitably get hybridised with each other (as well as with other extended states(97, 96)) and form extended states, according to the renormalisation-group procedure developed in Refs. (116, 117, 118) [see also Ref. (42)]. A Weyl semimetal in the presence of a random gauge field is another example of a system where the conventional analysis of rare regions cannot be applied(106) and awaits further studies.

6. POTENTIAL FOR EXPERIMENTAL REALISATION

Despite extensive theoretical studies, non-Anderson disorder-driven transitions still remain to be observed experimentally. In what follows we consider various systems that have the potential for observing such transitions.

6.1. Weyl and 3D Dirac semimetals

3D Weyl and Dirac semimetals ($\alpha = 1$) are currently among the most experimentally accessible systems in the high-dimensional regime ($3 = d > 2\alpha = 2$).

6.1.1. Solid-state semimetals. Recently 3D Dirac quasiparticles have been found experimentally in Na_3Bi (10) and Cd_3As_2 (11). WSMs have been discovered in $TaAs$ (13, 14, 17), TaP (15) and $NbAs$ (16).

While there are many types of disorder in solid-state systems, transport in realistic materials is typically dominated by charged impurities. In Weyl and Dirac semimetals, the disorder correlation length is given by the impurity screening length, $\lambda \sim v/[\alpha^{1/2} \max(\mu, T)]$, where $\alpha = \frac{e^2}{v\kappa}$ is the “fine-structure constant” and μ is the characteristic chemical potential [determined at low doping by the fluctuations of the impurity concentration(43)]. Because in realistic WSM materials $\alpha \lesssim 1$, this screening length exceeds the characteristic electron

wavelength $\lambda_e \sim v/\max(\mu, T)$ that determines the WSM conductivity. Because the observation of the non-Anderson disorder-driven transitions requires that the random potential be short-range (compared to the electron wavelength), these transitions cannot be observed in transport(43, 102, 119, 120, 121, 122, 123, 124, 125).

However, even in the presence of Coulomb impurities the transition can be observed in the DoS of doped systems(123). Indeed, the momentum states near a WSM node below the Fermi energy have large wavelengths that exceed the screening length λ set by the Fermi energy. Although such states do not contribute to conduction, they can be probed, for example in ARPES experiments, revealing the critical behaviour of the DoS at the transition near the node, which was discussed in Sec. 3.2.

6.1.2. Weyl and Dirac semimetals in cold-atomic systems and photonic crystals. Theoretical activity on Weyl semimetals has also spurred numerous proposals for realising Weyl and Dirac semimetals in controllable ultracold atomic gases [see, for example, Refs. (126, 127, 128, 129, 130, 131, 132, 133)]. Moreover, it has been demonstrated(134) that excitations with Weyl dispersion exist in all 3D systems of dipolar particles in the presence of magnetic field. Although cold-atomic 3D Weyl (Dirac) semimetals still remain to be realised, such systems are a promising platform for observing the physics of non-Anderson disorder-driven transitions. In particular, such systems allow one to realise short-ranged disorder potentials whose strength is readily controlled in experiment.

Recently a WSM has been realised(17) in a photonic crystal, a periodic structure with a broken inversion symmetry exposed to microwave radiation. Systems of such type allow for the controlled inclusion of short-range disorder and thus present another flexible platform for studying high-dimensional non-Anderson disorder-driven transitions.

6.2. 1D and 2D arrays of ultracold trapped ions

Arrays of trapped ultracold ions with long-range spin interactions $\propto 1/r^{d+\alpha}$ have recently been realised in 1D(45, 46, 47, 48) and 2D(49) lattices in magnetic traps, with a tunable parameter α . In a strong magnetic field, the propagation of single-spin-flip excitations in these systems is effectively a single-particle problem, with the particle dispersion $\epsilon_{\mathbf{k}} \propto k^\alpha$.

When α is tuned to values $\alpha < d/2$, these systems correspond to the case of high dimensions. When also subject to a weak disorder (e.g. a spatially random magnetic field), such systems present a flexible platform(44) for observing non-Anderson disorder-driven transitions. Similarly to the case of solid-state systems, arrays of trapped ions with $\alpha < d/2$ display the critical behaviour of the DoS and other observables, as discussed in Sec. 3 [the numerical results(44) for the critical behaviour of the DoS in a 1D chiral chain are shown in Fig. 9].

We note that current experiments with 1D chains(46) use relatively small numbers ($N \leq 16$) of ions, that may be insufficient for accurate observations of the transition. An additional difficulty is the accurate detection of the finite energy E_c of the critical point. This difficulty, however, could be overcome in chiral systems(44) with the quasiparticle dispersion $\epsilon_{\mathbf{k}} \propto |k|^\alpha \text{sign } k$, where the symmetry ensures $E_c = 0$, although such chiral systems still remain to be designed and realised. It is likely that observing high-dimensional non-Anderson transitions will require longer chains of trapped ions or using 2D arrays [which currently contain(49) approximately 300 ions].

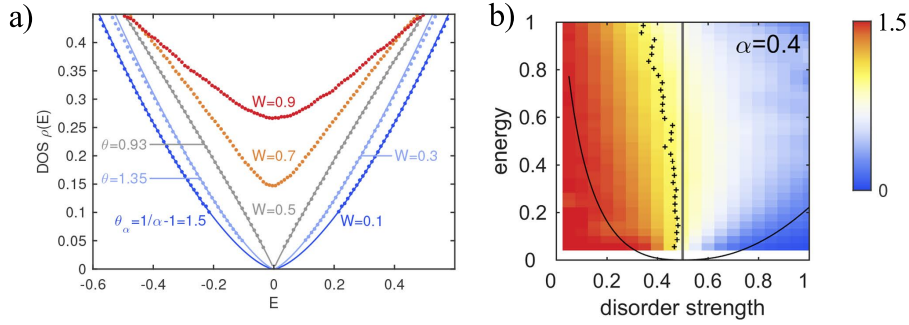


Figure 9

[Adapted from Ref. (44)] The critical behaviour of the density of states in a chiral 1D chain with the quasiparticle dispersion $\epsilon_k = |k|^\alpha \text{sign } k$, calculated numerically in Ref. (44). a) DoS as a function of energy. For subcritical disorder the DoS vanishes $\propto E^{\frac{d}{\alpha}-1}$ near $E = 0$. For supercritical disorder the low-energy DoS is nonzero. At the critical disorder $\rho(E) \propto E^{\frac{d}{\alpha}-1}$ b) Critical behaviour of the DoS on the diagram energy vs. disorder strength; the colour shows the exponent $\theta = \frac{\partial \ln \rho}{\partial \ln E}$.

6.3. Chiral superconductors

Another class of systems with the potential to realise high-dimensional disorder-driven transitions are 3D nodal superconductors. Such systems generically have points and/or lines on the Fermi surface where the superconducting gap vanishes. They are thus described by Bogolyubov-de-Gennes Hamiltonians with nodal quasiparticles of the form considered in this review, e.g., chiral $p_x \pm ip_y$ superconductors that host Weyl excitations. Therefore, such systems can be expected to display the non-Anderson disorder-driven transitions (provided superconductivity is not destroyed by disorder), that can be detected, e.g., in the quasiparticle density of states. These transitions in 3D chiral superconductors deserve further investigation.

At present, the existence of 3D chiral superconductors is not completely established, but there is evidence for their existence in several candidate materials (see Ref. (135) for review). A prominent example here is the candidate d -wave superconductor URu_2Si_2 (136, 137, 138, 139).

6.4. Quantum kicked rotors

The dynamics of a quantum rotor kicked by perturbations with d incommensurate frequencies can be mapped onto the problem of localisation of a quadratically dispersive particle in d dimensions in a (quasi-)random potential(53, 54). Thus, such systems may be used to study localisation phenomena and disorder-driven transitions, both Anderson and non-Anderson, in various dimensions. Quantum kicked rotors have been realised in systems of cold-atoms exposed to pulsed laser beams to demonstrate localisation in 1D systems(50) and the Anderson localisation transition in 3D(51, 52). These systems may be used similarly to demonstrate non-Anderson disorder-driven transitions in $d > 4$ dimensions and to study the properties of these transitions.

6.5. Numerical simulations in high dimensions

Numerical simulations allow access to all dimensions d , including those above the physical ($d = 1, 2, 3$), and thus can serve as another platform for the investigation of high-dimensional non-Anderson transitions. Often numerical simulations are carried out for models on lattices, which always have finite bands and quadratic particle dispersion $\epsilon_{\mathbf{k}} \propto k^2$ near band edges. Non-Anderson disorder-driven transitions can therefore be observed in such systems in dimensions $d > 4$ near band edges, however, so far the studies(55, 56, 57, 58, 59) of high-dimensional localisation phenomena focussed in states in the middle of the band and on the usual Anderson-transition criticality. Also, transport in disordered systems with arbitrary quasiparticle dispersion $\epsilon \propto k^\alpha$ may be simulated in momentum space using the scattering-matrix approach(25, 30, 106), which allows one to study non-Anderson disorder-driven transitions for arbitrary α and $d > 2\alpha$.

7. OPEN QUESTIONS AND FUTURE PROBLEMS

Below we list questions that in our view constitute some important further research directions related to the unconventional high-dimensional disorder-driven physics.

Interactions, magnetic field and more general disorder and band structures. A natural further research direction is the inclusion of electron-electron interactions and the study of its interplay with disorder. Recently such an interplay has been studied for Dirac semimetals in Refs. (20) and (140), however, a number of open questions remain, particularly, a more detailed analysis of physical observables. Also, most of the focus in the literature has been on potential disorder, while more generic disorder (random gauge field, random mass, etc.) is expected(66, 60) to appear.

Furthermore, recent studies have demonstrated [see, e.g., Ref. (141)] the existence of more general band structures, such as line nodes, some appearing in the context of chiral superconductors. The role of generic disorder for a variety of nodal band structures in the presence of interactions and, in particular, their effects on the unconventional disorder-driven transition remains an open problem. Another future direction of research is the interplay of the high-dimensional disorder-driven physics with magnetic field.

Interplay of rare-region and perturbative effects. In our view, it currently remains an open question whether the non-Anderson transitions discussed here are true phase transitions or sharp crossovers. This question requires the development of a field-theoretical description of disordered systems that accounts for the interplay of perturbative and rare-region effects.

As discussed in Sec. 5, rare-region effects are qualitatively distinct in systems that allow for localisation (semiconductors, Dirac semimetals, non-chiral chains of atoms, etc.) and systems where localisation is forbidden by symmetry and topology (chiral chains, single-node Weyl semimetals).

Models of infinite-dimensional systems ($d \rightarrow \infty$). Because the unconventional disorder-driven physics discussed in this review emerges in sufficiently high dimensions, it is natural to expect manifestations of this physics in random regular graphs and tree-like structures, which have been used to study the properties of the Anderson localisation transition in large and infinite dimensions [see, e.g., Refs. (142, 143, 144, 145, 146)].

Novel candidate materials. Systems that exhibit non-Anderson transitions and/or high-dimensional disorder-driven physics are probably not limited to those discussed in this review and shown in Fig. 1.

We believe that the possibility of observing these effects in other types of systems deserves further investigation. Apparent candidates include, but are not limited to, excitations in interacting systems near quantum phase transitions (e.g. the superconductor-insulator transition), photonic systems and phonons in disordered materials.

DISCLOSURE STATEMENT

The authors are not aware of any affiliations, memberships, funding, or financial holdings that might be perceived as affecting the objectivity of this review.

ACKNOWLEDGMENTS

We are grateful to M. Gärttner, A.M. Ostrovsky, A.M. Rey, Ya.I. Rodionov, B. Sbierski, B. Skinner and especially V. Gurarie for collaboration on the subjects of this review and to R. Nandkishore, B. Normand, T. Ohtsuki, A. Prem, B. Sbierski and M. Schütt for comments on the manuscript. We are also deeply indebted to B. Normand for the proofreading of the manuscript and numerous suggestions and to B. Skinner for insightful discussions of the review. Our work was supported financially by NSF grants DMR-1001240, DMR-1205303, PHY-1211914, PHY-1125844 and PHY-1125915. LR also acknowledges a Simons Investigator award from the Simons Foundation and the hospitality of the Kavli Institute of Theoretical Physics where a part of this work was completed.

LITERATURE CITED

1. Anderson PW. 1958. *Phys. Rev.* 109:1492
2. Basko DM, Aleiner IL, Altshuler BL. 2006. *Ann. Phys.* 321:1126
3. Abrikosov AA. 1988. *Fundamentals of the theory of metals.* Oxford: Elsevier
4. Abrikosov AA, Gorkov LP, Dzyaloshinski IE. 1975. *Methods of quantum field theory in statistical physics.* New York: Dover
5. Efetov KB. 1999. *Supersymmetry in disorder and chaos.* New York: Cambridge University Press
6. Fradkin E. 1986. *Phys. Rev. B* 33:3263
7. Fradkin E. 1986. *Phys. Rev. B* 33:3257
8. Young SM, Zaheer S, Teo JCY, Kane CL, Mele EJ, Rappe AM. 2012. *Phys. Rev. Lett.* 108:140405
9. Wang Z, Sun Y, Chen XQ, Franchini C, Xu G, et al. 2012. *Phys. Rev. B* 85:195320
10. Liu ZK, Zhou B, Zhang Y, Wang ZJ, Weng HM, et al. 2014. *Science* 343:864
11. Liu ZK, Jiang J, Zhou B, Wang ZJ, Zhang Y, et al. 2014. *Nature Mat.* 13:677
12. Wan X, Turner AM, Vishwanath A, Savrasov SY. 2011. *Phys. Rev. B* 83:205101
13. Huang SM, Xu SY, Belopolski I, Lee CC, Chang G, et al. 2015. *Nature Comm.* 6:7373
14. Xu SY, Belopolski I, Alidoust N, Neupane M, Bian G, et al. 2015. *Science* 349:6248
15. Xu SY, Belopolski I, Sanchez DS, Zhang C, Chang G, et al. 2015. *Sci. Adv.* 1:1501092
16. Xu SY, Alidoust N, Belopolski I, Yuan Z, Bian G, et al. 2015. *Nat. Phys.* 11:748
17. Lv BQ, Weng HM, Fu BB, Wang XP, Miao H, et al. 2015. *Phys. Rev. X* 5:031013
18. Shindou R, Murakami S. 2009. *Phys. Rev. B* 79:045321
19. Ryu S, Nomura K. 2012. *Phys. Rev. B* 85:155138
20. Goswami P, Chakravarty S. 2011. *Phys. Rev. Lett.* 107:196803

21. Kobayashi K, Ohtsuki T, Imura KI, Herbut IF. 2014. *Phys. Rev. Lett.* 112:016402
22. Ominato Y, Koshino M. 2014. *Phys. Rev. B* 89:054202
23. Syzranov SV, Radzihovsky L, Gurarie V. 2015. *Phys. Rev. Lett.* 114:166601
24. Syzranov SV, Gurarie V, Radzihovsky L. 2015. *Phys. Rev. B* 91:035133
25. Sbierski B, Pohl G, Bergholtz EJ, Brouwer PW. 2014. *Phys. Rev. Lett.* 113:026602
26. Pixley JH, Goswami P, Das Sarma S. 2015. *Phys. Rev. Lett.* 115:076601
27. Pixley JH, Goswami P, Das Sarma S. 2016. *Phys. Rev. B* 93:085103
28. Chen CZ, Song J, Jiang H, Sun Q, Wang Z, Xie XC. 2015. *Phys. Rev. Lett.* 115:246603
29. Liu S, Ohtsuki T, Shindou R. 2016. *Phys. Rev. Lett.* 116:066401
30. Sbierski B, Bergholtz EJ, Brouwer PW. 2015. *Phys. Rev. B* 92:115145
31. Shapourian H, Hughes TL. 2016. *Phys. Rev. B* 93:075108
32. Bera S, Sau JD, Roy B. 2016. *Phys. Rev. B* 93:201302
33. Syzranov SV, Ostrovsky PM, Gurarie V, Radzihovsky L. 2016. *Phys. Rev. B* 93:155113
34. Pixley JH, Huse DA, Das Sarma S. 2016. *Phys. Rev. X* 6:021042
35. Roy B, Das Sarma S. 2016. *Phys. Rev. B* 93:119911
36. Roy B, Juricic V, Das Sarma S. 2016. *Sci. Rep.* 6:32446
37. Syzranov SV, Gurarie V, Radzihovsky L. 2016. *Ann. Phys.* 373:694
38. Louvet T, Carpentier D, Fedorenko AA. 2016 arXiv:1605.02009
39. Pixley JH, Huse DA, Das Sarma S. 2016. *Phys. Rev. B* 94:121107
40. Wegner F. 1981. *Z. Phys. B* 44:9
41. Suslov IM. 1994. *Sov. Phys. JETP* 79:307
42. Nandkishore R, Huse DA, Sondhi SL. 2014. *Phys. Rev. B* 89:245110
43. Skinner B. 2014. *Phys. Rev. B* 90:060202(R)
44. Gärttner M, Syzranov SV, Rey AM, Gurarie V, Radzihovsky L. 2015. *Phys. Rev. B* 92:041406(R)
45. Richerme P, Gong ZX, Lee A, Senko C, Smith J, et al. 2014. *Nature Lett.* 511:198
46. Islam R, Senko C, Campbell WC, Korenblit S, Smith J, et al. 2013. *Science* 340:583
47. Jurcevic P, Lanyon BP, Hauke P, Hempel C, Zoller P, et al. 2014. *Nature* 511:202
48. Jurcevic P, Hauke P, Maier C, Hempel C, Lanyon BP, et al. 2015. *Phys. Rev. Lett.* 115:100501
49. Britton JW, Sawyer BC, Keith AC, Wang CCJ, Freericks JK, et al. 2012. *Nature Lett.* 484:489
50. Moore FL, Robinson JC, Bharucha C, Williams PE, Raizen MG. 1994. *Phys. Rev. Lett.* 73:2974
51. Chabé J, Lemarié G, Grémaud B, Delande D, Szafrangis P, Garreau JC. 2008. *Phys. Rev. Lett.* 101:255702
52. Lemarié G, Chabé J, Szafrangis P, Garreau JC, Grémaud B, Delande D. 2009. *Phys. Rev. A* 80:043626
53. Grepel DR, Prange RE, Fishman S. 1984. *Phys. Rev. A* 29:1639
54. Casati G, Guarneri I, Shepelyansky DL. 1989. *Phys. Rev. Lett.* 62:345
55. Markos P. 2006. *Acta Physica Slovaca* 56:561
56. Garcia-Garcia AM, Cuevas E. 2007. *Phys. Rev. B* 75:174203
57. Ueoka Y, Slevin K. 2014. *J. Phys. Soc. Jpn.* 83:084711
58. Zharekshv IK, Kramer B. 1998. *Ann. Phys. (Leipzig)* 7:442
59. Slevin K, Ohtsuki T. 2016. *J. Phys. Soc. Jpn.* 85:104712
60. Aleiner IL, Efetov KB. 2006. *Phys. Rev. Lett.* 97:236801
61. Ostrovsky PM, Gornyi IV, Mirlin AD. 2006. *Phys. Rev. B* 74:235443
62. Gell-Mann M, Low FE. 1954. *Phys. Rev.* 95:1300
63. Wilson KG. 1965. *Phys. Rev.* 140:B445
64. Sachdev S. 2005. Quantum phase transitions. Cambridge: Cambridge University Press
65. Dotsenko VS, Dotsenko VS. 1983. *Adv. Phys.* 32:129
66. Ludwig AWW, Fisher MPA, Shankar R, Grinstein G. 1994. *Phys. Rev. B* 50:7526
67. Bocquet M, Serban D, Zirnbauer M. 2000. *Nucl. Phys. B* 578:628
68. Altland A, Simons BD, Zirnbauer MR. 2002. *Phys. Rep.* 359:283

69. Guruswamy S, LeClair A, Ludwig A. 2000. *Nucl. Phys. B* 583:475
70. Efetov KB, Larkin AI, Khmel'nitskii DE. 1980. *Sov. Phys. JETP* 52:568
71. Belitz D, Kirkpatrick TR. 1994. *Rev. Mod. Phys.* 66:261
72. Kamenev A. 2011. *Field theory of non-equilibrium systems*. Cambridge: Cambridge Univ. Press
73. de Gennes PG. 1979. *Scaling concepts in polymer physics*. Ithaca, New York: Cornell University Press
74. Singh KK. 1975. *Phys. Rev. B* 12:2819
75. Singh KK. 1978. *Phys. Rev. B* 17:324
76. Uzunov DI. 1981. *Phys. Lett.* 87A:11
77. Radzihovsky L, Park J, Weichman P. 2004. *Phys. Rev. Lett.* 92:160402
78. Romans MWJ, Duine RA, Sachdev S, Stoof HTC. 2004. *Phys. Rev. Lett.* 93:020405
79. Radzihovsky L, Weichman PB, Park JI. 2008. *Ann. Phys.* 323:2376
80. Nikolić P, Sachdev S. 2007. *Phys. Rev. A* 75:033608
81. Veillette MY, Sheehy DE, Radzihovsky L. 2007. *Phys. Rev. A* 75:043614
82. Gurarie V, Radzihovsky L. 2007. *Ann. Phys.* 322:2
83. Syzranov SV, Moor A, Efetov KB. 2012. *Phys. Rev. Lett.* 108:256601
84. Syzranov SV, Yevtushenko OM, Efetov KB. 2012. *Phys. Rev. B* 86:241102(R)
85. Gross DJ, Neveu A. 1974 10:3235
86. Wetzel W. 1985. *Phys. Lett.* 153B:297
87. Ludwig AWW. 1987. *Nucl. Phys. B* 285:97
88. Bondi A, Curci G, Paffuti G, Rossi P. 1990. *Ann. Phys.* 199:268
89. Gracey JA. 1990. *Nucl. Phys. B* 341:403
90. Tracas ND, Vlachos ND. 1990. *Phys. Lett.* 236:333
91. Luperini C, Rossi P. 1991. *Ann. Phys.* 212:371
92. Kivel NA, Stepanenko AS, Vasilev AN. 1994. *Nucl. Phys. B* 424:619
93. Ludwig AWW, Wiese KJ. 2003. *Nucl. Phys. B* 661:577
94. Gracey JA, Luthe T, Schroder Y. 2016. arXiv:1609.05071
95. Schuessler A, Ostrovsky PM, Gornyi IV, Mirlin AD. 2009. *Phys. Rev. B* 79:075405
96. Mott N. 1987. *J. Phys. C: Solid State Phys.* 20:3075
97. Mott NF. 1967. *Adv. Phys.* 16:49
98. Bulka B, Schreiber M, Kramer B. 1987. *Z. Phys. B* 66:21
99. Ryu S, Schnyder A, Furusaki A, Ludwig A. 2010. *New J. Phys.* 12:065010
100. Nielsen HB, Ninomiya M. 1981. *Nuclear Physics B* 185:20
101. Lu HZ, Shen SQ. 2015. *Phys. Rev. B* 92:035203
102. Burkov AA, Hook MD, Balents L. 2011. *Phys. Rev. B* 84:235126
103. Hosur P, Parameswaran SA, Vishwanath A. 2012. *Phys. Rev. Lett.* 108:046602
104. Altland A, Bagrets D. 2015. *Phys. Rev. Lett.* 114:257201
105. Altland A, Bagrets D. 2016. *Phys. Rev. B* 93:075113
106. Sbierski B, Decker KSC, Brouwer PW. 2016. *Phys. Rev. B* 94:220202(R)
107. Evers F, Mirlin AD. 2008. *Rev. Mod. Phys.* 80:1355
108. Wegner F. 1980. *Z. Phys. B* 36:209
109. Foster MS. 2012. *Phys. Rev. B* 85:085122
110. Chou YZ, Foster MS. 2014. *Phys. Rev. B* 89:165136
111. Lifshitz IM. 1963. *Sov. Phys. JETP* 17:1159
112. Zittartz J, Langer JS. 1966. *Phys. Rev.* 148:741
113. Halperin BI, Lax M. 1966. *Phys. Rev. Lett.* 148:722
114. Lifshits IM, Gredeskul SA, Pastur LA. 1988. *Introduction to the theory of disordered systems*. New York: Wiley
115. Yaida S. 2016. *Phys. Rev. B* 93:075120
116. Levitov LS. 1990. *Ann. Phys.* 5:507

117. Levitov LS. 1990. *Phys. Rev. Lett.* 64:547
118. Levitov LS. 1989. *Europhys. Lett.* 9:83
119. Ominato Y, Koshino M. 2015. *Phys. Rev. B* 91
120. Das Sarma S, Hwang EH, Min H. 2015. *Phys. Rev. B* 91:035201
121. Lundgren R, Laurell P, Fiete GA. 2014. *Phys. Rev. B* 90:165115
122. Ramakrishnan N, Milletari M, Adam S. 2015. *Phys. Rev. B* 92:245120
123. Rodionov YI, Syzranov SV. 2015. *Phys. Rev. B* 91:195107
124. Pesin DA, Mishchenko EG, Levchenko A. 2015. *Phys. Rev. B* 92:174202
125. Klier J, Gornyi IV, Mirlin A. 2015. *Phys. Rev. B* 92:205113
126. Lan Z, Goldman N, Bermudez A, Lu W, Öhberg P. 2011. *Phys. Rev. B* 84:165115
127. Jiang JH. 2012. *Phys. Rev. A* 85:033640
128. Anderson BM, Juzeliūnas G, Galitski VM, Spielman IB. 2012. *Phys. Rev. Lett.* 108:235301
129. Dubček T, Kennedy CJ, Lu L, Ketterle W, Soljačić M, Buljan H. 2015. *Phys. Rev. Lett.* 114:225301
130. Ganeshan S, Das Sarma S. 2015. *Phys. Rev. B* 91:125438
131. Liu B, Li X, Yin L, Liu WV. 2015. *Phys. Rev. Lett.* 114:045302
132. Lepori L, Fulga IC, Trombettoni A, Burrello M. 2016. *Phys. Rev. B* 94:085107
133. Lepori L, Fulga IC, Trombettoni A, Burrello M. 2016. *Phys. Rev. A* 94:053633
134. Syzranov SV, Wall ML, Zhu B, Gurarie V, Rey AM. 2015. arXiv:1512.08723
135. Kallin C, Berlinsky J. 2016. *Rep. Prog. Phys.* 79:054502
136. Yano K, Sakakibara T, Tayama T, Yokoyama M, Amitsuka H, et al. 2008. *Phys. Rev. Lett.* 100:017004
137. Kasahara Y, Shishido H, Shibauchi T, Haga Y, Matsuda TD, et al. 2009. *New J. Phys.* 11:055061
138. Schemm ER, Baumbach RE, Tobash PH, Ronning F, Bauer ED, Kapitulnik A. 2015. *Phys. Rev. B* 91:140506(R)
139. Kang J, Fernandes RM. 2015. *Phys. Rev. B* 92:054504
140. Moon EG, Kim YB. 2014. arXiv:1409.0573
141. Xie LS, Schoop LM, Seibel EM, Gibson QD, Xie W, Cava RJ. 2015. *APL Mat.* 3:083602
142. Abou-Chacra R, Anderson PW, Thouless DJ. 1973. *J. Phys. C: Solid State Phys* 6:1734
143. Mirlin AD, Fyodorov YV. 1991. *Nucl. Phys. B* 366:507
144. Mirlin AD, Fyodorov YV. 1994. *Phys. Rev. Lett.* 72:526
145. Mard HJ, Hoyos JA, Miranda E, Dobrosavljević V. 2014. arXiv:1412.3793
146. Tikhonov KS, Mirlin AD, Skvortsov MA. 2016. arXiv:1604.05353